


Acoustic Behavior of a Dense Suspension in an Inhomogeneous Flow in a Microchannel

A. Nath and A.K. Sen^{*}

Department of Mechanical Engineering, Indian Institute of Technology Madras, Chennai, 600036, India

 (Received 27 May 2019; revised manuscript received 3 August 2019; published 5 November 2019)

We report the behavior of a dense suspension (blood sample, $\varphi > 0.1$) coflowing with an aqueous buffer in a microchannel exposed to an acoustic standing wave studied by experiments and a theoretical model. The coupled effect of acoustophoretic particle migration and bulk relocation due to an inhomogeneous-fluid configuration leads to interesting phenomena. Our study reveals that depending on the acoustic impedance of the suspension (Z_s) and buffer (Z_b) streams, different flow regimes (complete relocation, acoustic migration, nonrelocation and nonmigration, and partial relocation) can be observed. The occurrence of different regimes is explained by the impedance contrast (i.e., ΔZ_{sb} and ΔZ_{pb}) and is characterized in terms of the particle residence (τ_{res}), acoustic relocation (τ_{rel}), and acoustic migration (τ_{mig}) timescales. We discover the partial-relocation regime, wherein acoustic migration of particles results in a band of a highly concentrated suspension at the suspension-buffer interface that alone relocates to the pressure node. The partial-relocation regime thus offers a technique for acoustic-driven splitting of a suspension stream into denser and diluted suspension streams.

DOI: [10.1103/PhysRevApplied.12.054009](https://doi.org/10.1103/PhysRevApplied.12.054009)

I. INTRODUCTION

Acoustic manipulation of particles, fluids, and suspensions has profound applications in the field of microfluidics [1,2]. The effect of acoustic forces on fluid systems has been well studied, and different phenomena, such as the radiation force on particles within a medium [3], the force acting at the interface of two miscible or immiscible fluids [4–6], and acoustic streaming [7], have been investigated. The acoustic radiation force acting on particles has been used to sort [8–11] and separate cells [12,13], bacteria [14–17], exosomes [18], and other biomolecules [19].

When a fluid system with parallel coflowing miscible fluids of different density was subjected to an acoustic bulk standing wave directed perpendicular to the interface, it was observed that a bulk radiation force acts at the interface between the streams for a difference in acoustic impedance even as low as 0.1% [20]. This results in a final stable configuration that will have the stream with higher acoustic impedance at the pressure node. Remarkably, an interesting feature of such an inhomogeneous system of fluids is the confinement of acoustic streaming rolls to a region near the wall [21] until the system inhomogeneity is reduced by diffusion and later advection [22]. Concentration gradients have been used to introduce inhomogeneity in the system and to evaluate the compressibility of circulating tumor cells [23], separate bacteria from blood

[24], and separate circulating tumor cells from peripheral blood [25]. The suppression of acoustic streaming in the case of inhomogeneous systems has enabled effective size-based separation of particles by inducing acoustic relocation, which drags only the smaller particles along with the relocating stream [26].

The development of microfluidic devices for point-of-care diagnostics requires rapid separation of different components of blood [27,28]. Previous studies using bulk acoustic waves relied on focusing the cells to the pressure node and extracting blood plasma from the sides. Shear-induced diffusion in the case of a dense suspension was shown to counteract the acoustophoretic focusing once the minimum achievable width had been obtained [29], which introduces a limit on the throughput. Inertial separation of red blood cells (RBCs) from undiluted blood by shear-induced diffusion shows that separation can be achieved with a higher throughput although with a much longer focusing length [30]. A central saline solution was flanked by undiluted blood at a trifurcated inlet. Introducing a similar configuration at the inlet and subjecting the streams to acoustophoretic force can supplement the inertial focusing and provide higher throughput. However, it may be difficult to extract cells from whole blood into a central buffer solution as even a small difference in acoustic impedance between the two streams may rapidly lead to bulk relocation of the streams as noted earlier for two different liquid solutions, albeit without the presence of particles [31]. This problem is usually circumvented by working

^{*}ashis@iitm.ac.in

with diluted blood [28] to ensure that the impedance of the blood streams is lower than that of the central buffer stream. However, this limitation imposed on the use of a dense suspension [32] (volume fraction $\varphi > 0.1$; e.g., whole blood) as the side streams motivated the present work.

Here we study the acoustic behavior of a dense suspension as side streams coflowing with a central buffer stream in a microchannel. Our experiments and simulations reveal that the relocation behavior of a suspension differs markedly from that of a system of solutions (without particles). In the case of an inhomogeneous system of solutions with a concentration gradient or coflowing streams with unmatched acoustic impedance, with a low-impedance stream at the center or the nodal plane, the full relocation proceeds with a gradual broadening of the higher-impedance side streams to enclose the entire channel width and subsequent bulk transport to the pressure node to obtain the final configuration [20]. With the high-impedance stream at the node, the interface broadening is arrested due to suppression of streaming, and broadening occurs only due to diffusion. However, in the case of a suspension in an inhomogeneous-fluid configuration, the coupled effect of acoustophoretic migration of particles and bulk relocation of the suspension leads to complex but interesting phenomena. Depending on the acoustic impedance of the particles, suspension, and buffer, different regimes (complete relocation, acoustic migration, nonrelocation and nonmigration, and partial migration) are observed. The occurrence of the different regimes is explained in terms of impedance contrast of particles and the suspension with respect to the buffer and is characterized in terms of important timescales: particle residence, acoustic migration and acoustic relocation timescales. The partial-relocation regime is studied in detail.

II. THEORY

The radiation forces acting on a rigid spherical particle in the presence of an acoustic field are well established in the literature [33]. For a one-dimensional planar standing half-wave, the dominant primary acoustic radiation force acting on a compressible sphere (of radius a) can be written as [33]

$$F = 4\pi\phi(\tilde{\kappa}, \tilde{\rho})ka^3E_{ac} \sin 2ky, \quad (1)$$

where the acoustic contrast factor $\phi = (1/3)[(5\tilde{\rho} - 2)/(2\tilde{\rho} + 1) - \tilde{\kappa}]$, with $\tilde{\rho} = \rho_p/\rho_f$ and $\tilde{\kappa} = \kappa_p/\kappa_f$ denoting the particle-to-fluid ratios of density and compressibility, respectively, k is the wave number, and acoustic energy density $E_{ac} = p_a^2/(4\rho_0c_0^2)$, where p_a is the pressure amplitude within the channel and ρ_0 and c_0 are the average density and speed of sound, respectively. Positive and negative values of the acoustic contrast factor indicate

that the acoustic radiation force acts toward the pressure node and antinode, respectively. The acoustic contrast factor of RBCs in blood is positive [34]; thus, the primary radiation force gives rise to migration of cells toward the node at the center of the channel. In the presence of an acoustic field, in addition to the primary radiation force, the effect of scattering of the primary acoustic field by a particle in a pair of particles leads to a secondary force. However, generally, the secondary radiation force is approximately 2 orders of magnitude smaller [35] than the primary radiation force and for a particle in a homogeneous suspension the mean interparticle force is zero owing to a symmetrical distribution [36]. For acoustic migration of particles, the primary radiation force is equated with the drag force to obtain an expression for the acoustophoretic mobility, which is used to solve the particle-flux equation in the numerical model.

The radiation force acting at the interface of coflowing streams was studied recently and it was shown that it arises from nonzero divergence in the time-averaged momentum-flux-density tensor owing to variations of density and compressibility between the two streams [5]. The expression for the acoustic force density acting on an inhomogeneous fluid was obtained as

$$\mathbf{f}_{ac} = -\frac{1}{4}|p_1^2|\nabla\kappa - \frac{1}{4}|\mathbf{v}_1^2|\nabla\rho, \quad (2)$$

where p_1 and \mathbf{v}_1 refer to the homogeneous acoustic pressure and velocity fields, respectively. Here we express the acoustic force density in terms of the local acoustic impedance ($Z = \rho c$), where ρ is the density of the medium and c is the speed of sound in the medium (see Sec. III in Supplemental Material [37]). For weak spatial variation of the local density, speed of sound, and hence acoustic impedance, we obtain

$$\mathbf{f}_{ac} = -E_{ac} \left[\cos(2ky) \nabla \hat{Z} - \nabla \hat{c} \right]. \quad (3)$$

Here the nondimensional acoustic impedance \hat{Z} and speed of sound \hat{c} are defined on the basis of $Z = Z_0(1 + \hat{Z})$ and $c = c_0(1 + \hat{c})$, where Z_0 and c_0 refer to average initial values in the cross section.

In addition to acoustic relocation force, for suspensions, the effect arising from hydrodynamic interaction between particles and the fluid needs to be considered. Any particle dragged through the suspending fluid due to acoustophoretic force exerts an opposite reaction force that tends to drag the suspending fluid along with it [31,32,38]. The net reaction force on the fluid depends on the number of particles per unit volume $\varphi/(4\pi a^3/3)$, where φ is the volume fraction, and the acoustic force on the particle F ,

giving

$$\mathbf{f}_b = \frac{\varphi}{\frac{4}{3}\pi a^3} F. \quad (4)$$

In an initial configuration, with impedance of the central stream (buffer) higher than that of the suspension (side stream), that is, $Z_b > Z_s$, the interfacial radiation force \mathbf{f}_{ac} helps in stabilizing the fluid interface against hydrostatic pressure, which tends to stratify the streams horizontally. However, when the impedance of the central stream (buffer) is lower than that of the suspension (side stream), that is, $Z_b < Z_s$, due to the aforementioned radiation force, bulk relocation of the fluids is initiated due to small perturbations at the interface, and in the final configuration, the fluid with the higher acoustic impedance is relocated to the center.

III. NUMERICAL MODELING

For numerical modeling of dense suspensions in the present case, since the ratio of the particle size to the width of the channel $a/W < 0.2$ (the radius of a RBC is taken as $a = 2.8 \mu\text{m}$), the continuum description is found to be valid [39]. The governing equations are formulated on the basis of the mixture model as described in a previous study [40] and are solved in the finite-element-based solver COMSOL MULTIPHYSICS (version 5.3). The continuous phase for the present case is taken to be a mixture of blood plasma and iodixanol, and the local variation of different properties in each third of the cross section [i.e., I and II in Fig. 1(b)]

is incorporated in the model in terms of spatial functions (see Sec. III in Supplemental Material [37]).

To simulate the migration-relocation phenomena involving a dense suspension of solid particles (RBCs) dispersed in a continuous phase (blood plasma) and acoustic radiation force in an inhomogeneous medium, the following equations are used. The continuity equation is written as

$$\frac{\partial \rho}{\partial t} + \nabla \cdot (\rho \mathbf{u}) = 0, \quad (5)$$

with volume-averaged density $\rho = \varphi_p \rho_p + (1 - \varphi_p) \rho_l$ and velocity $\mathbf{u} = c_p \mathbf{u}_p + (1 - c_p) \mathbf{u}_l$, where φ_i and c_i represent the volume fraction and the mass fraction of the dispersed and continuous phases indicated with subscripts p and l , respectively. The slip velocity, defined as $\mathbf{u}_{\text{slip}} = (\mathbf{u}_p - \mathbf{u}_l)$, is used in the formulation.

The momentum equation is given as

$$\begin{aligned} \rho \frac{\partial \mathbf{u}}{\partial t} + \rho (\mathbf{u} \cdot \nabla) \mathbf{u} = & -\nabla p - \nabla \cdot [\rho c_p (1 - c_p) \mathbf{u}_{\text{slip}} \cdot \mathbf{u}_{\text{slip}}] \\ & + \nabla \cdot [\eta (\nabla \mathbf{u} + (\nabla \mathbf{u})^T)] \\ & + \rho \mathbf{g} + \mathbf{f}_{ac} + f_h \mathbf{f}_b, \end{aligned} \quad (6)$$

where p is the pressure, η is the shear viscosity, \mathbf{f}_{ac} is the acoustic force density, and \mathbf{f}_b is the net reaction force from particles on the suspending fluid, which is multiplied here by a factor defined below as the hindering function (f_h). The hindering function accounts for decreased mobility owing to the presence of a large number of particles [41,42] and consequently the effect of the relocation force

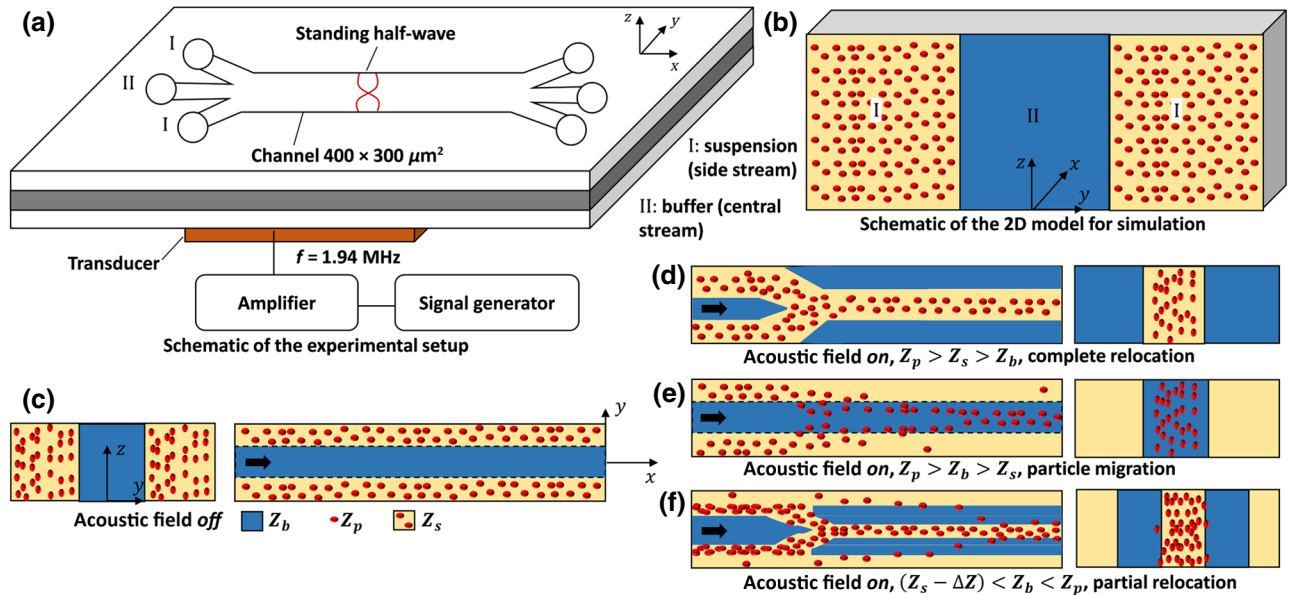


FIG. 1. (a) The microchannel through-etched in silicon wafer and anodically bonded to glass lids of 500- μm depth. The piezoelectric transducer is actuated after signal amplification. (b) The simulation model with a two-dimensional (2D) computational domain of size $375 \times 150 \mu\text{m}^2$. (c)–(f) The different flow regimes.

on the fluid outweighs the hydrodynamic effect. For the general case, $f_h \mathbf{f}_b / \mathbf{f}_{ac} = [3\phi k \sin(2ky) f_h \varphi] / \nabla \hat{Z} \cos(2ky - 1) \sim 10^{-2}$ (i.e., the relocation force is 2 orders larger).

The acoustophoretic, diffusive, and gravitational effects on the motion of solid particles are modeled with use of the particle-flux equation. The relation between particle flux and slip velocity is given as $\mathbf{u}_{\text{slip}} = \mathbf{J}_p / [\varphi_p \rho_p (1 - c_p)]$, where \mathbf{J}_p is the particle flux, which is defined as follows:

$$\mathbf{J}_p / \rho_p = - \left[\varphi_p D_\varphi \nabla (\gamma \varphi_s) + \varphi_p^2 \gamma D_\eta \nabla (\ln \eta) \right] + f_h \mathbf{u}_{\text{st}} \varphi + f_h \mathbf{u}_{\text{ac}} \varphi, \quad (7)$$

where $D_\varphi = 0.41a^2$ and $D_\eta = 0.62a^2$ are the values chosen for the diffusion constants [43] and $f_h = \eta_l (1 - \varphi_{\text{av}})^2 / \eta$ is the hindering function, where φ_{av} is the average volume fraction in the suspension (here $\varphi_{\text{av}} = 0.46$). By equating the gravitational force and the drag force, we determine the settling velocity as $\mathbf{u}_{\text{st}} = (2/9\eta_l)[a^2(\rho_p - \rho_l)\mathbf{g}]$. Similarly, by equating the primary acoustic radiation force [Eq. (1)] and the drag force, we determine the acoustophoretic mobility as $\mathbf{u}_{\text{ac}} = (2/3\eta_l)(a^2 E_{\text{ac}} \phi k \sin 2k)$. For a dense suspension, the local viscosity η will depend on the local volume fraction φ , which can be represented with the different correlations available in the literature [44]. In our model, we use the Krieger-Dougherty viscosity relation [45], for which the relative effective shear viscosity (i.e., the ratio of the viscosity of the suspension η to that of the particle-free suspending fluid η_l) is given as

$$\frac{\eta}{\eta_l} = \left(1 - \frac{\varphi}{\varphi_{\text{max}}} \right)^{-2.5\varphi_{\text{max}}}, \quad (8)$$

where φ_{max} is the maximum packing fraction, which is taken as 0.8 to account for the deformability of RBCs.

The transport of local iodixanol concentration s is modeled with the convection-diffusion equation [Eq. (9)], where $D = 0.8 \times 10^{-10} \text{ m}^2/\text{s}$ is the diffusion coefficient of iodixanol solution. The iodixanol concentration field and the volume fraction of particles alter the local values of density, viscosity, and the speed of sound in the system, and this is modeled in terms of defined functions [23,46,47] from previous studies (see Supplemental Material [37]):

$$\frac{\partial s}{\partial t} + \nabla \cdot (\mathbf{u}s) = -\nabla \cdot (-D\nabla s). \quad (9)$$

In our simulations, we take the channel cross section as $400 \times 300 \mu\text{m}^2$ [see Fig. 1(b)] and because of the inherent symmetry in the problem, we consider only one half ($y > 0$) of the channel cross section for simulation. The four outer boundaries of the entire domain represent the microfluidic no-slip hard-wall ($\mathbf{u} = 0$) boundary condition. To simulate the different regimes, different initial and

operating conditions in terms of iodixanol concentration, volume fraction of the side stream (suspension), flow rate, acoustic impedance of the central and side streams, and the fluid properties are used.

The acoustic energy densities used in our simulations are obtained through experiments as described in Sec. IV [48]. The acoustic energy densities depend on the actuation frequencies and the pair of fluids. At resonance, the highest acoustic energy density E_{ac} is experimentally measured to be 113.2 J/m^3 , which is used in the simulations. For all simulations, initially, the side stream (i.e., region I) is occupied by a dense suspension (blood, $\varphi = 0.46$). The acoustic impedance of the central stream (i.e., region II) is varied to obtain the different relocation phenomena. After performing mesh convergence analysis, we choose a computational mesh consisting of 37 056 triangular elements. The simulations are performed until the solutions converge to steady-state configurations in all cases. The numerical model is validated for the case of an inhomogeneous solution (see Supplemental Material [37]).

IV. EXPERIMENTS

A glass-silicon-glass microchip with trifurcated inlets and outlets is used for the current study; a schematic of the setup is presented in Fig. 1(a). The microfluidic channels are through-etched in a silicon wafer of $300\text{-}\mu\text{m}$ depth by deep reactive-ion etching and bonded to glass lids of $500\text{-}\mu\text{m}$ thickness on both sides by anodic bonding. The dimensions of the main channel are $W = 400 \mu\text{m}$, $H = 300 \mu\text{m}$, and $L = 20 \text{ mm}$. The inlet and outlet holes are drilled through the top glass lid to facilitate fluidic access. The suspension and buffer are introduced into the microchannel device through polymer tubes by our connecting the inlet and outlet ports to syringe pumps (neMESYS pump, Cetoni, Germany). Undiluted blood ($\varphi = 0.46$) is infused through the side inlets for all experiments, while the buffer solution infused through the central inlet is varied to observe the different regimes. A piezoelectric transducer (Sparkler Ceramics, India) of 1-mm thickness is glued to the bottom glass lid and the system is actuated by an rf signal generated by a function generator (SMC100A, Rohde & Schwarz, Germany) and an amplifier (75A250A, Amplifier Research, USA). The power input in our experiments ranges from 60 mW to 4.0 W.

To find the resonant frequency of the system, polystyrene beads (Sigma-Aldrich, Bangalore, India) of size $10 \pm 0.2 \mu\text{m}$ are introduced into the system and the actuation frequency is varied over the range 1.85–2.05 MHz. At the resonant frequency in half-wave mode, the beads remain at the nodal plane at the center of the channel, which is found to be 1.93 MHz. To measure the acoustic energy density at different applied voltages, the particle-tracking method is used [48]. The suspension is prepared by our adding a small concentration of $10 \pm$

0.2 μm polystyrene beads to a medium with 9% iodixanol in phosphate-buffered saline (PBS), ensuring the beads remain neutrally buoyant. First, the resonant frequency is verified by our focusing the spatially distributed particles to the central nodal plane. Then, with the acoustic field turned *off*, a small quantity of suspension is injected into the channel, ensuring that the beads again remain uniformly distributed in the channel. With the acoustic field turned *on*, the particle migration to the pressure node is captured with a high-speed camera (SA5, Photron, United Kingdom) at a frame rate of 250 frames/s. Equating the acoustophoretic and drag forces acting on a particle yields the following relation for the particle location:

$$y(t) = \frac{1}{k_y} \tan^{-1} \left[\tan[k_y y(0)] \exp \left(\frac{4\phi(\tilde{\kappa}, \tilde{\rho})}{9\eta(k_y a)^2 E_{ac} t} \right) \right]. \quad (10)$$

From the experimental videos, the location of the particle y during migration with time t is obtained with the program Tracker (Open Source Physics). Using the above relation, we compute the acoustic energy density E_{ac} for different actuation voltages. The acoustic energy density approximately ranges from 10 to 110 J/m^3 , and the highest acoustic energy density obtained is $113.2 \pm 4.1 \text{ J}/\text{m}^3$.

For each experiment, the buffer is prepared by our adding the density-gradient medium, iodixanol solution (OptiPrep, Sigma-Aldrich, Bangalore, India), to 1X PBS. OptiPrep is chosen in this study because of its high ratio of acoustic impedance to viscosity [23]. The blood sample is freshly drawn and collected in Vacutainer tubes (BD Biosciences, San Jose, CA, USA) containing ethylenediamine tetraacetic acid (EDTA) as an anticoagulant from healthy volunteers at the institute hospital (Indian Institute of Technology Madras, Chennai, India) after the required ethical clearance is obtained. The blood sample is used as is without any dilution, and all the experiments are performed within 2 h of the blood being drawn. Rhodamine B solution is added to either the central stream or the side (blood) streams for flow visualization, ensuring that the change in the acoustic impedance is negligible and does not affect the relocation-migration behavior. A small concentration of 0.5 vol% 30-mM Rhodamine B provided adequate contrast despite the large number of background cells present in blood. The properties of the different components, whole-blood suspension, blood plasma, and blood cells, and the acoustic-contrast-factor calculations [49–52] are presented in Sec. II in Supplemental Material [37]. An epifluorescence microscope (IX71, Olympus Corporation, Japan) with a high-speed CCD camera (SA5, Photron, United Kingdom) and a 130-W reflected-light mercury burner is used for flow visualization, and the images are taken at a location close to the outlet (approximately 20 mm from the inlet) and analyzed with ImageJ (National Institutes of Health, USA). While capturing fluorescent images, we

focus at the middle of the channel ($z = H/2$) so that fluorescence can be collected as evenly as possible throughout the height [53].

V. RESULTS AND DISCUSSION

Depending on the concentration of iodixanol in the central buffer stream, different characteristics are observed [see Figs. 1(c)–1(f)]. Figures 2 and 3 show experimental and simulation results, respectively, for the different regimes; namely, complete-relocation, particle-migration, and partial-relocation regimes. The complete-relocation regime [Figs. 1(d), 2(a), and 3(a)] is observed with undiluted blood with particle volume fraction $\phi = 0.46$ as the side stream, buffer with 15% iodixanol concentration as the central stream, flow rates of the suspension stream (side stream) of 20 $\mu\text{l}/\text{min}$ and the buffer stream of 200 $\mu\text{l}/\text{min}$, and energy density $E_{ac} = 113.2 \text{ J}/\text{m}^3$. The acoustic impedances of the suspension and buffer streams are $Z_s = 1.67 \text{ MPa s}/\text{m}$ and $Z_b = 1.62 \text{ MPa s}/\text{m}$, respectively, and the acoustic impedance of the particles (blood cells) is $Z_p = 1.81 \text{ MPa s}/\text{m}$. Since $Z_p > Z_s > Z_b$ (Fig. 4), one would expect that acoustic bulk relocation of the suspension stream or acoustic migration of the blood cells toward the pressure node would occur. However, since the relocation timescale is shorter than the acoustic migration timescale (discussed later) owing to the dominant bulk relocation force, the entire suspension stream relocates to the pressure node located at the center of the channel. In Fig. 2(a), the suspension streams, which are indicated by the dark regions on both sides of the channel, relocate to the center of the channel, and consequently the buffer stream (bright region since it is mixed with fluorescent dye) relocates to the sides. The complete relocation of the suspension stream is further verified by our measuring the variation of the fluorescence intensity across the channel, which shows the low-fluorescence-intensity suspension region has completely migrated to the center of the channel. The time evolution of complete relocation of the suspension stream (with $\phi = 0.46$) with respect to the volume fraction of suspended particles and the concentration of iodixanol obtained from simulations is depicted in Fig. 3(a).

Figures 2(b) and 3(b) [and the schematic in Fig. 1(e)] show the particle-migration regime (nonrelocation) observed with undiluted blood with particle volume fraction $\phi = 0.46$ as the side streams, buffer with 30% iodixanol as the central stream, flow rates of the suspension (side stream) of 20 $\mu\text{l}/\text{min}$ and the buffer of 100 $\mu\text{l}/\text{min}$, and energy density $E_{ac} = 113.2 \text{ J}/\text{m}^3$. Here the acoustic impedance of the buffer stream Z_b is 1.73 $\text{MPa s}/\text{m}$. Since $Z_p > Z_b > Z_s$ (see Fig. 4), the particles are subjected to primary radiation force and migrate toward the pressure node at the center of the channel. Since the buffer stream has higher acoustic impedance than the suspension stream,

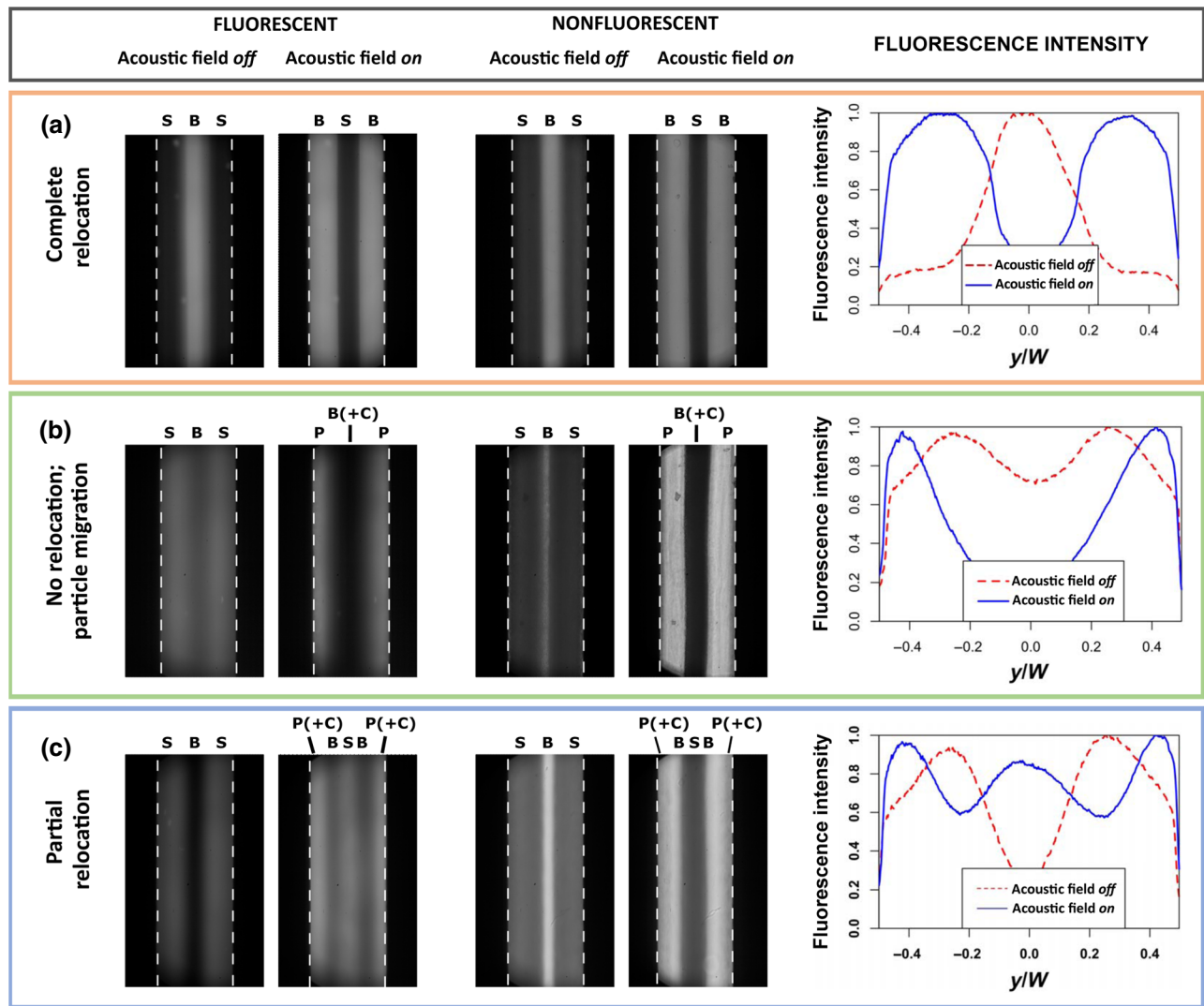


FIG. 2. (a) Experimental images showing complete relocation. Variation of intensity obtained from line scanning with ImageJ confirms complete relocation. The acoustic impedances of the suspension and buffer streams are $Z_s = 1.67$ MPa s/m and $Z_b = 1.62$ MPa s/m, respectively, and the acoustic impedance of the particles (RBCs) is $Z_p = 1.81$ MPa s/m. (b) Nonrelocation of the streams with particle migration from the side suspension to the central buffer, $Z_b = 1.73$ MPa s/m. (c) Partial relocation of the side suspension to the center, $Z_b = 1.68$ MPa s/m. The nonfluorescent image reveals a very-dilute nonrelocated suspension close to the walls, indicated as P(+C). The fluorescent tracer is added to the buffer in (a) and the suspension in (b),(c). The acoustic energy density E_{ac} is 113.2 J/m³ for all cases. The dashed lines in white highlight the channel walls, and the different streams are indicated by S for the suspension, B for the buffer, P for plasma, and C for blood cells.

no bulk relocation of the suspension stream is observed. When the buffer has an even-higher iodixanol concentration (i.e., more than 45% in the central stream), we observe a nonrelocation-and-nonmigration regime since $Z_b > Z_p > Z_s$. In this case, since the RBCs have a negative acoustic contrast with respect to the buffer, acoustophoretic migration of the blood cells into the central stream does not occur.

The partial-relocation regime [Figs. 2(c), 3(c), and 1(f)] is observed with undiluted blood having particle volume fraction $\phi = 0.46$ as the side stream and buffer with 18%–25% iodixanol concentration as the central stream.

The images show partial relocation observed with a central buffer with 22% iodixanol, for which the acoustic impedance Z_b is 1.68 MPa s/m. The flow rates of the suspension stream (side stream) and the buffer stream are 20 and 200 μ l/min, respectively, and the energy density E_{ac} is 113.2 J/m³. Since $Z_b \approx Z_s < Z_p$ (see Fig. 4), no relocation is observed at the beginning but as $Z_p > Z_{plasma}$, the particles (blood cells) present in the suspension stream migrate within the suspension stream toward the interface. However, because of higher impedance of the buffer stream compared with the plasma and a large particle volume fraction, the acoustic migration of particles from

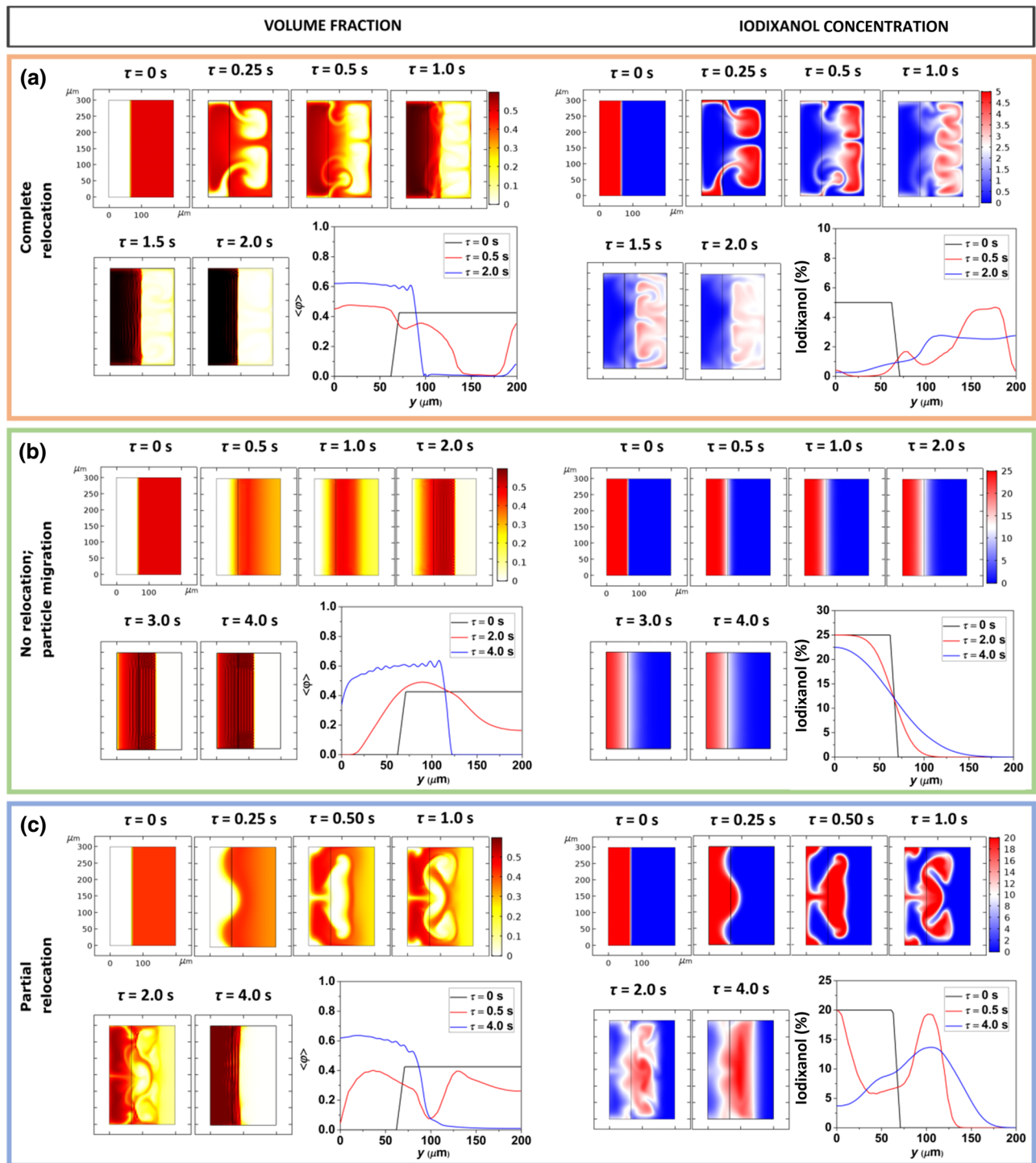


FIG. 3. Variation of the particle volume fraction and the local iodixanol concentration in the cross section for (a) complete relocation of the suspension stream, (b) no relocation, and (c) partial relocation. Results are presented for only one half of the cross section ($y > 0$) due to inherent symmetry.

the interface toward the pressure node is suppressed. The particles migrating from the suspension toward the center accumulate near the suspension-buffer interface. Thus, a highly concentrated band of particles (blood cells) is formed at the interface, and when $Z_s > Z_b$ is satisfied, the

highly concentrated band alone relocates to the pressure node at the center of the channel and gets separated from the low-concentration suspension stream at the wall. So the original suspension stream splits into a highly concentrated stream that relocates to the center of the channel and

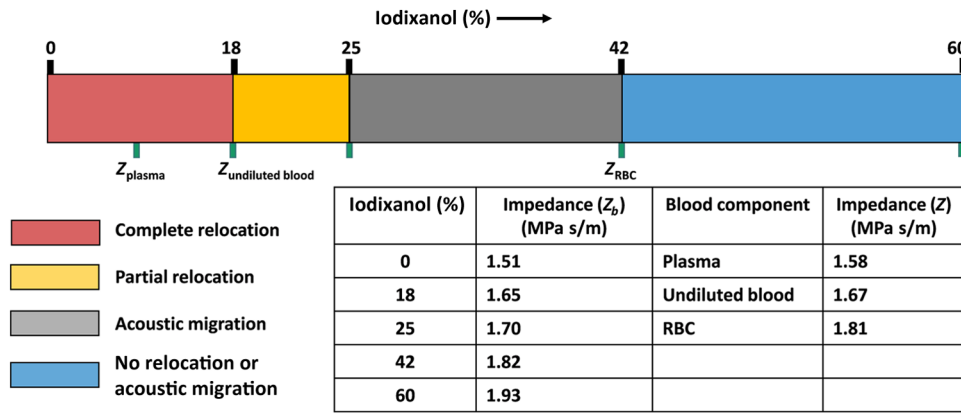


FIG. 4. The different relocation regimes observed for different acoustic impedances of the central stream (i.e., phosphate-buffered saline with different percentages of iodixanol). Also, the acoustic impedances for different concentrations of iodixanol and for different components of blood are tabulated [23,49,54].

a low-concentration stream that continues to flow close to the wall, revealing the partial-relocation regime. With sufficient residence time (or a longer channel for the same flow rates), all the particles are eventually focused at the center.

Next we discuss the importance of the different timescales involved and illustrate the different regimes in terms of the relevant timescales. The lateral migration of suspended particles in a dense suspension is driven by the combined effect of acoustics and shear-induced diffusion [29]. The acoustophoretic migration timescale τ_{mig} , that is, the time taken by a particle to traverse a distance $\Delta y = y(t) - y(0)$, is calculated with the following equation (which is derived by equating the acoustic radiation force on a particle to the corresponding Stokes drag force [33]):

$$\tau_{\text{mig}} = \frac{3}{4\phi} \frac{c_0^2}{\omega^2 a^2} \frac{\eta_l}{f_h E_{\text{ac}}} \ln \left(\frac{\tan[ky(t)]}{\tan[ky(0)]} \right). \quad (11)$$

The shear-induced-diffusion timescale is obtained as $\tau_{\text{SID}} = W^2 / (13.6\phi\gamma_{\text{av}}a^2)$, where γ_{av} is the average shear rate at the interface between the side stream and the central stream [55]. Using a Poiseuille-flow profile, for a homogeneous fluid with total flow rate $Q = 240 \mu\text{l}/\text{min}$, we obtain $\tau_{\text{SID}} \sim 27$ s. The actual flow profile in the channel will be blunter owing to the shear-thinning effect of the blood suspension [30] and hence γ_{av} will have a lower value and τ_{SID} can be even higher.

The molecular-diffusion timescale is expressed as $\tau_D = (W/3)^2/D$, where D can be taken as the larger of the diffusion coefficients of the working fluids, blood or iodixanol. For the present case, the diffusion constants are on the order of 10^{-10} , and for $D = 0.8 \times 10^{-10} \text{ m}^2/\text{s}$ (for iodixanol solution), the diffusion timescale $\tau_D \sim 350$ s.

The residence timescale, which indicates the amount of time for which a particle resides within the acoustic field, is given as

$$\tau_{\text{res}} = \frac{LWH}{Q}, \quad (12)$$

where L and H are the channel length and height, respectively.

The timescale associated with acoustic relocation (τ_{rel}) is computed experimentally by our tracking the variation of fluorescence intensities across different sections along the length of the channel. Once the system attains a stable configuration, the fluorescence-intensity profiles do not show any marked variation further downstream. The calculations of the timescales for different cases are detailed in Sec. VII in Supplemental Material [37]. Our calculations show that τ_{mig} , τ_{rel} , and τ_{res} are on the order of 1 s. Since τ_{SID} and τ_D are much greater than the other timescales, the effects of shear-induced diffusion and molecular diffusion are safely ignored.

The different relocation regimes [Figs. 1(d)–1(f)] are explained by our using the acoustophoretic migration and bulk relocation timescales, disregarding shear-induced and molecular diffusion. In the complete-relocation regime, with particle volume fraction $\phi = 0.46$, buffer with 15% iodixanol concentration as the central stream, flow rates of the suspension stream (side stream) of $20 \mu\text{l}/\text{min}$ and the buffer stream of $200 \mu\text{l}/\text{min}$, and energy density $E_{\text{ac}} = 113.2 \text{ J}/\text{m}^3$, the acoustic relocation timescale $\tau_{\text{rel}} \sim 0.1$ s, acoustic migration timescale $\tau_{\text{mig}} \sim 1.23$ s, and residence timescale $\tau_{\text{res}} \sim 0.60$ s. Since $\tau_{\text{rel}} \ll \tau_{\text{mig}}$, relocation is a much-faster process compared with acoustic migration, and thus the suspension stream completely relocates to the center of the channel.

In the acoustic migration regime, with $\phi = 0.46$, buffer with 30% iodixanol as the central stream, flow rates of the suspension (side stream) of $20 \mu\text{l}/\text{min}$ and the buffer of $100 \mu\text{l}/\text{min}$, and energy density $E_{\text{ac}} = 113.2 \text{ J}/\text{m}^3$, the acoustic relocation timescale τ_{rel} can arbitrarily be taken to be very long ($\tau_{\text{rel}} \gg 1$ s) as the configuration remains unfavorable to relocation, the acoustic migration timescale $\tau_{\text{mig}} \sim 1.23$ s, and the residence timescale $\tau_{\text{res}} \sim 1.03$ s. Since $\tau_{\text{mig}} \ll \tau_{\text{rel}}$, the particles migrate completely toward the pressure node, and relocation of the suspension stream is not observed. In the nonrelocation-and-nonmigration regime, with $\phi = 0.46$, buffer with more than 45% iodixanol as the central stream, flow rates of

the suspension (side stream) of $20 \mu\text{l}/\text{min}$ and the buffer of $100 \mu\text{l}/\text{min}$, and energy density $E_{ac} = 113.2 \text{ J}/\text{m}^3$, the acoustic relocation timescale will be very long ($\tau_{rel} \gg 1 \text{ s}$) due to an unfavorable configuration similarly to the migration regime, and the acoustic migration timescale τ_{mig} will be very long ($\tau_{mig} \gg 1 \text{ s}$) as the particle can traverse from the side suspension only to the side-center interface due to a change in sign of the contrast factor in the central buffer stream. Here the residence timescale $\tau_{res} \sim 0.97 \text{ s}$, and since $\tau_{res} < \tau_{mig}$ and $\tau_{res} < \tau_{rel}$, we observe neither particle migration to the buffer nor relocation of streams.

In the partial-relocation regime, with $\phi = 0.46$, buffer with 22% iodixanol as the central stream, flow rates of the suspension (side stream) of $20 \mu\text{l}/\text{min}$ and the buffer of $100 \mu\text{l}/\text{min}$, and energy density $E_{ac} = 113.2 \text{ J}/\text{m}^3$, before initiation of the relocation, the time taken for a particle to traverse to the interface is calculated to be $\tau_{mig} \sim 1.23 \text{ s}$, whereas the acoustic relocation timescale τ_{rel} remains arbitrarily long ($\tau_{rel} \gg 1 \text{ s}$) as the configuration is unfavorable. Since $\tau_{mig} \ll \tau_{rel}$, the particles migrate toward the interface and relocation of the suspension stream is not observed. Because of hindered mobility of the particles owing to a large number of neighbors, the local particle concentration close to the interface rises, increasing the local acoustic impedance relative to the buffer. When the high-concentration band is formed, the relocation timescale now attains a finite value, $\tau_{rel} \ll 1 \text{ s}$, which depends on the local impedance at the interface, while the migration timescale $\tau_{mig} \sim 1 \text{ s}$. Since $\tau_{rel} < \tau_{mig}$, the

high-concentration-suspension band relocates to the center. Thus, the relocation to obtain the final configuration here involves an initial particle migration followed by bulk transport of the high-impedance band to the center. For a system with buffer having 22% iodixanol concentration as the central stream with flow rates of the suspension stream (side stream) of $20 \mu\text{l}/\text{min}$ and the buffer stream of $200 \mu\text{l}/\text{min}$, and energy density $E_{ac} = 113.2 \text{ J}/\text{m}^3$, the total relocation time is computed from experimental results (see Supplemental Material [37]) to be $\tau_{rel} \sim 0.38 \text{ s}$. We see that the total residence timescale $\tau_{res} > \tau_{rel}$, which also needs to be satisfied to observe the partial-relocation regime.

Next we discuss the dynamic evolution of the partial-relocation phenomenon. It is extremely challenging to estimate the local changes in particle volume fraction from experiments, and thus we rely on numerical simulations to understand the partial-relocation mechanism. In the partial-relocation regime, the spatial variation of acoustic impedance [normalized as $(Z - Z_0)/Z_0$] across the channel cross section with time is shown in Fig. 5(a). Before application of the acoustic field (at $\tau = 0 \text{ s}$), there is a sharp jump in the acoustic impedance across the suspension-buffer (or, side-stream–central-stream) interface. The acoustic impedances of the suspension stream and the central stream are 1.66 and $1.70 \text{ MPa s}/\text{m}$, respectively. When the acoustic field is turned *on*, the profile at $\tau = 0.3 \text{ s}$ shows a decrease in the acoustic impedance in the suspension stream closer to the wall and an increase

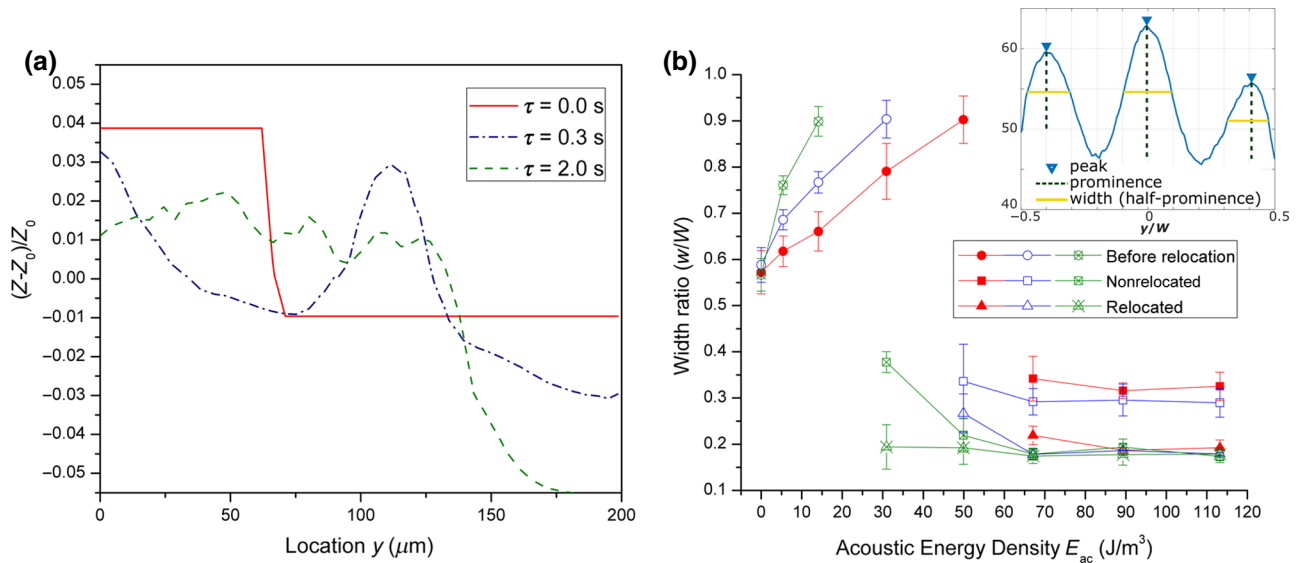


FIG. 5. (a) Spatial variation of the acoustic impedance across the channel cross section with time (shown for half the cross section with $y > 0$) for the case of partial relocation. (b) Effects of operating conditions, flow rates of the suspension and buffer streams, and acoustic energy density on the partial-relocation behavior with regard to the observed width ratio (a statistical average based on three measurements is shown). The ratio of the central-buffer flow rate to total side-suspension flow rate is maintained as $Q_b/Q_s = 5$ for all cases [filled red symbols, $Q_b = 100 \mu\text{l}/\text{min}$ and $Q_s = 20 \mu\text{l}/\text{min}$; unfilled blue symbols, $Q_b = 200 \mu\text{l}/\text{min}$ and $Q_s = 40 \mu\text{l}/\text{min}$; crossed green symbols, $Q_b = 300 \mu\text{l}/\text{min}$ and $Q_s = 60 \mu\text{l}/\text{min}$]. The inset shows measurements of the central relocated width and total nonrelocated width at the sides from the fluorescence-intensity profile.

in acoustic impedance around the interface. This can be attributed to the fact that since $Z_b \approx Z_s < Z_p$ is satisfied, as discussed earlier, there is continuous migration of blood cells from the suspension stream toward the interface and thus the blood-cell concentration decreases closer to the wall and increases at the interface. The particle agglomeration at the interface forms a highly concentrated band of cells, thus increasing the local acoustic impedance. When the acoustic impedance in this concentrated band exceeds that of the central buffer (i.e., $Z > Z_b$), the concentrated band of blood cells relocates to the center. In the final stable configuration at $\tau = 2$ s, the acoustic impedance at the central region of the cross section is higher than at the sides.

Further, we experimentally investigate the effects of operating conditions, flow rates of the suspension and buffer streams, and energy density on the partial-relocation behavior, as shown in Fig. 5(b). The widths of the relocated and nonrelocated streams are computed from the corresponding fluorescence-intensity signal by our measuring the width at half-prominence [56] after signal smoothing [57] (see Sec. VI in Supplemental Material [37] for more details). For a suspension (undiluted blood) flow rate of $20 \mu\text{l}/\text{min}$ at each side and a buffer (22% iodixanol, impedance $1.68 \text{ MPa s}/\text{m}$) flow rate of $200 \mu\text{l}/\text{min}$ at the center [unfilled symbols in Fig. 5(b)], it is observed that with increasing E_{ac} up to a critical energy density $E_{ac} = 40 \text{ J}/\text{m}^3$, the suspension stream gradually broadens (i.e., the suspension width increases linearly) until it occupies the entire width of the channel. The broadening of the suspension is experimentally observed and measured from the fluorescence profile (using Rhodamine B in blood). The broadening of the suspension stream is attributed to initiation of lateral bulk transport of the suspension along the bottom of the channel.

Beyond the critical energy density, $E_{ac} = 40 \text{ J}/\text{m}^3$, the suspension stream undergoes partial relocation and gets split into a high-concentration stream that relocates to the center of the channel and a low-concentration stream that continues to stay close to the channel wall. The widths of the high-concentration relocated stream and low-concentration nonrelocated stream with increasing energy density are presented. It is observed that with an increase in the energy density, there is small decrease in the widths occupied by the relocated and nonrelocated streams. However, beyond $E_{ac} \sim 90 \text{ J}/\text{m}^3$, the differences are minimal and the relocated and nonrelocated suspension streams remain with constant width. So it can be taken that the widths of the relocated and nonrelocated streams are independent of the acoustic energy density, while a critical energy density is required to observe the partial-relocation regime. Thus, for a suspension initially occupying width $w_s = 0.58W$ of the channel (with the central buffer occupying the remaining width $w_b = 0.42W$), part of the suspension stream of width $w_r = 0.18W$ would relocate and

occupy the central portion of the channel, whereas the other part of the stream of width $w_{nr} = 0.32W$ (on both sides) would remain close to the channel walls. For the same flow-rate ratio, a decrease in the flow rates results in an increase in the critical energy density to $E_{ac} = 50 \text{ J}/\text{m}^3$ as shown in Fig. 5(b). With higher suspension and buffer flow rates, it is observed that the suspension stream broadens more rapidly to occupy the entire width of the channel before relocation to the center. The width of the relocated stream at the center is nearly independent of the flow rates, while the width of the nonrelocated suspension stream at the side reduces with increasing suspension and buffer flow rates.

VI. CONCLUSION

We study the acoustic behavior of a dense suspension coflowing as side streams with an aqueous buffer as the central stream in a microchannel. We find that the behavior of dense suspensions is markedly different from that of acoustic migration of a dense or dilute suspension in a homogeneous-fluid configuration as well as for pure solutions in an inhomogeneous-fluid configuration reported previously. The particle migration due to a suspension and bulk relocation due to an inhomogeneous-fluid configuration are intertwined and thus reveal interesting effects. Depending on the operating conditions (acoustic impedance contrast of the suspension and buffer streams, flow rates, and energy densities) four different regimes [complete relocation (no migration), acoustic migration (no relocation), nonrelocation and nonmigration, and partial relocation] are observed. Numerical simulations based on a mixture model show that the partial-relocation regime is observed due to initial acoustic migration of particles toward the suspension-buffer interface followed by relocation of the high-concentration band of particles to the pressure node at the center. The four different regimes are illustrated on the basis of the impedance contrast of the particles and the suspension and buffer streams and are characterized on the basis of the different timescales. The complete-relocation regime is observed for $\tau_{rel} < \tau_{mig} < \tau_{res}$, acoustic migration is observed for $\tau_{mig} < \tau_{res} < \tau_{rel}$, and the nonrelocation-and-nonmigration regime is observed for $\tau_{res} < \tau_{mig}$ and $\tau_{res} < \tau_{rel}$. For intermediate impedance differences between the buffer and the suspension, the relocation is observed to be only partial and proceeds through a combined migration-relocation process. The partial-relocation regime offers a technique for splitting a suspension stream into two substreams, one stream with a higher concentration and another stream with a lower concentration.

ACKNOWLEDGMENTS

A.K.S. thanks the Department of Science and Technology for providing financial support for the project

via Grant No. DST/SJF/ETA-03/2017-18. The support of the Centre for NEMS and Nanophotonics, Indian Institute of Technology Madras, for device fabrication is acknowledged.

- [1] T. Laurell, F. Petersson, and A. Nilsson, Chip integrated strategies for acoustic separation and manipulation of cells and particles, *Chem. Soc. Rev.* **36**, 492 (2007).
- [2] J. Friend and L. Y. Yeo, Microscale acoustofluidics: Microfluidics driven via acoustics and ultrasonics, *Rev. Mod. Phys.* **83**, 647 (2011).
- [3] L. V. King, On the acoustic radiation pressure on spheres, *Proc. Royal Soc. A* **147**, 212 (1934).
- [4] L. Landau and E. M. Lifshitz, *Fluid Mechanics* (Pergamon, New York, 1959).
- [5] J. T. Karlsen, P. Augustsson, and H. Bruus, Acoustic Force Density Acting on Inhomogeneous Fluids in Acoustic Fields, *Phys. Rev. Lett.* **117**, 1 (2016).
- [6] E. Hemachandran, S. Karthick, T. Laurell, and A. K. Sen, Relocation of coflowing immiscible liquids under acoustic field in a microchannel, *EPL* **125**, 54002 (2019).
- [7] S. J. Lighthill, Acoustic streaming, *J. Sound Vib.* **61**, 391 (1978).
- [8] F. Petersson, L. Åberg, A. M. Swärd-Nilsson, and T. Laurell, Free flow acoustophoresis: Microfluidic-based mode of particle and cell separation, *Anal. Chem.* **79**, 5117 (2007).
- [9] O. Jakobsson, C. Grenvall, M. Nordin, M. Evander, and T. Laurell, Acoustic actuated fluorescence activated sorting of microparticles, *Lab Chip* **14**, 1943 (2014).
- [10] X. Ding, S.-C. S. Lin, B. Kiraly, H. Yue, S. Li, I.-K. Chiang, J. Shi, S. J. Benkovic, and T. J. Huang, On-chip manipulation of single microparticles, cells, and organisms using surface acoustic waves, *Proc. Natl. Acad. Sci. U.S.A.* **109**, 11105 (2012).
- [11] L. Schmid, D. A. Weitz, and T. Franke, Sorting drops and cells with acoustics: Acoustic microfluidic fluorescence-activated cell sorter, *Lab Chip* **14**, 3710 (2014).
- [12] C. Grenvall, C. Magnusson, H. Lilja, and T. Laurell, Concurrent isolation of lymphocytes and granulocytes using refocused free flow acoustophoresis, *Anal. Chem.* **87**, 5596 (2015).
- [13] Y. Chen, M. Wu, L. Ren, J. Liu, P. H. Whitley, L. Wang, and T. J. Huang, High-throughput acoustic separation of platelets from whole blood, *Lab Chip* **16**, 3466 (2016).
- [14] M. Antfolk, P. B. Muller, P. Augustsson, H. Bruus, and T. Laurell, Focusing of sub-micrometer particles and bacteria enabled by two-dimensional acoustophoresis, *Lab Chip* **14**, 2791 (2014).
- [15] P. Dow, K. Kotz, S. Gruszka, J. Holder, and J. Fiering, Acoustic separation in plastic microfluidics for rapid detection of bacteria in blood using engineered bacteriophage, *Lab Chip* **18**, 923 (2018).
- [16] P. Ohlsson, M. Evander, K. Petersson, L. Mellhammar, A. Lehmusvuori, U. Karhunen, M. Soikkeli, T. Seppä, E. Tuunainen, A. Spangar, P. Von Lode, K. Rantakokko-Jalava, G. Otto, S. Scheduling, T. Soukka, S. Wittfooth, and T. Laurell, Integrated acoustic separation, enrichment, and microchip polymerase chain reaction detection of bacteria from blood for rapid sepsis diagnostics, *Anal. Chem.* **88**, 9403 (2016).
- [17] B. Hammarström, T. Laurell, and J. Nilsson, Seed particle-enabled acoustic trapping of bacteria and nanoparticles in continuous flow systems, *Lab Chip* **12**, 4296 (2012).
- [18] M. Wu, Y. Ouyang, Z. Wang, R. Zhang, P.-H. Huang, C. Chen, H. Li, P. Li, D. Quinn, M. Dao, S. Suresh, Y. Sadovskiy, and T. J. Huang, Isolation of exosomes from whole blood by integrating acoustics and microfluidics, *Proc. Natl. Acad. Sci. U.S.A.* **114**, 10584 (2017).
- [19] C. Grenvall, P. Augustsson, J. R. Folkenberg, and T. Laurell, Harmonic microchip acoustophoresis: A route to online raw milk sample precondition in protein and lipid content quality control, *Anal. Chem.* **81**, 6195 (2009).
- [20] S. Deshmukh, Z. Brzozka, T. Laurell, and P. Augustsson, Acoustic radiation forces at liquid interfaces impact the performance of acoustophoresis, *Lab Chip* **14**, 3394 (2014).
- [21] J. T. Karlsen, W. Qiu, P. Augustsson, and H. Bruus, Acoustic Streaming and its Suppression in Inhomogeneous Fluids, *Phys. Rev. Lett.* **120**, 54501 (2018).
- [22] W. Qiu, J. T. Karlsen, H. Bruus, and P. Augustsson, Characterization of Acoustic Streaming in Gradients of Density and Compressibility, *Phys. Rev. Appl.* **10**, 1 (2018).
- [23] P. Augustsson, J. T. Karlsen, H. W. Su, H. Bruus, and J. Voldman, Iso-acoustic focusing of cells for size-insensitive acousto-mechanical phenotyping, *Nat. Commun.* **7**, 1 (2016).
- [24] P. Ohlsson, K. Petersson, P. Augustsson, and T. Laurell, Acoustic impedance matched buffers enable separation of bacteria from blood cells at high cell concentrations, *Sci. Rep.* **8**, 9156 (2018).
- [25] S. Karthick, P. N. Pradeep, K. Pandian, and A. Sen, Acoustic impedance based label-free isolation of circulating tumour cells from blood using acoustophoresis, *Lab Chip* **18**, 3802 (2018).
- [26] G. P. Gautam, R. Gurung, F. A. Fencel, and M. E. Piyasena, Separation of sub-micron particles from micron particles using acoustic fluid relocation combined with acoustophoresis, *Anal. Bioanal. Chem.* **410**, 6561 (2018).
- [27] M. Toner and D. Irimia, Blood-on-a-chip, *Annu. Rev. Biomed. Eng.* **7**, 77 (2005).
- [28] A. Lenshof, A. Ahmad-Tajudin, K. Järås, A. M. Swärd-Nilsson, L. Åberg, G. Marko-Varga, J. Malm, H. Lilja, and T. Laurell, Acoustic whole blood plasmapheresis chip for prostate specific antigen microarray diagnostics, *Anal. Chem.* **81**, 6030 (2009).
- [29] S. Karthick and A. Sen, Role of shear induced diffusion in acoustophoretic focusing of dense suspensions, *Appl. Phys. Lett.* **109**, 014101 (2016).
- [30] J. Zhou, C. Tu, Y. Liang, B. Huang, Y. Fang, X. Liang, I. Papautsky, and X. Ye, Isolation of cells from whole blood using shear-induced diffusion, *Sci. Rep.* **8**, 9411 (2018).
- [31] P. Augustsson and T. Laurell, Acoustofluidics 11: Affinity specific extraction and sample decomplexing using continuous flow acoustophoresis, *Lab Chip* **12**, 1742 (2012).
- [32] M. W. Ley and H. Bruus, Continuum modeling of hydrodynamic particle-particle interactions in microfluidic high-concentration suspensions, *Lab Chip* **16**, 1178 (2016).
- [33] H. Bruus, Acoustofluidics 7: The acoustic radiation force on small particles, *Lab Chip* **12**, 1014 (2012).

- [34] F. Petersson, A. Nilsson, C. Holm, H. Jönsson, and T. Laurell, Continuous separation of lipid particles from erythrocytes by means of laminar flow and acoustic standing wave forces, *Lab Chip* **5**, 20 (2005).
- [35] S. M. Woodside, B. D. Bowen, and J. M. Piret, Measurement of ultrasonic forces for particle-liquid separations, *AICHE J.* **43**, 1727 (1997).
- [36] G. T. Silva and H. Bruus, Acoustic interaction forces between small particles in an ideal fluid, *Phys. Rev. E* **90**, 063007 (2014).
- [37] See Supplemental Material at <http://link.aps.org/supplemental/10.1103/PhysRevApplied.12.054009> for details on the derivation of f_{ac} , calculation of the relocated width and computation of timescales from experimental data as well as more information on the experimental setup and device used.
- [38] C. Mikkelsen and H. Bruus, Microfluidic capturing-dynamics of paramagnetic bead suspensions, *Lab Chip* **5**, 1293 (2005).
- [39] H. Lei, D. A. Fedosov, B. Caswell, and G. E. Karniadakis, Blood flow in small tubes: Quantifying the transition to the non-continuum regime, *J. Fluid Mech.* **722**, 214 (2013).
- [40] R. Rao, L. Mondy, A. Sun, and S. Altobelli, A numerical and experimental study of batch sedimentation and viscous resuspension, *Int. J. Numer. Methods Fluids* **39**, 465 (2002).
- [41] J. Happel, Viscous flow in multiparticle systems: Slow motion of fluids relative to beds of spherical particles, *AICHE J.* **4**, 197 (1958).
- [42] H. M. Vollebregt, R. G. Van Der Sman, and R. M. Boom, Suspension flow modelling in particle migration and micro-filtration, *Soft Matter* **6**, 6052 (2010).
- [43] R. J. Phillips, R. C. Armstrong, R. A. Brown, A. L. Graham, and J. R. Abbott, A constitutive equation for concentrated suspensions that accounts for shear-induced particle migration, *Phys. Fluids* **4**, 30 (1992).
- [44] A. Dörr, A. Sadiki, and A. Mehdizadeh, A discrete model for the apparent viscosity of polydisperse suspensions including maximum packing fraction, *J. Rheol.* **57**, 743 (2013).
- [45] I. M. Krieger and T. J. Dougherty, A mechanism for non-Newtonian flow in suspensions of rigid spheres, *Trans. Soc. Rheol.* **3**, 137 (1959).
- [46] E. L. Bradley and J. Sacerio, The velocity of ultrasound in human blood under varying physiologic parameters, *J. Surg. Res.* **12**, 290 (1972).
- [47] A. S. Ahuja and W. R. Hende, Effects of particle shape and orientation on propagation of sound in suspensions, *J. Acoust. Soc. Am.* **63**, 1074 (1978).
- [48] R. Barnkob, P. Augustsson, T. Laurell, and H. Bruus, Measuring the local pressure amplitude in microchannel acoustophoresis, *Lab Chip* **10**, 563 (2010).
- [49] R. J. Trudnowski and R. C. Rico, Specific gravity of blood and plasma at 4 and 37 °C, *Clin. Chem.* **20**, 615 (1974).
- [50] A. H. Harker and J. A. Temple, Velocity and attenuation of ultrasound in suspensions of particles in fluids, *J. Phys. D* **21**, 1576 (1988).
- [51] R. J. Urick, A sound velocity method for determining the compressibility of finely divided substances, *J. Appl. Phys.* **18**, 983 (1947).
- [52] M. A. H. Weiser and R. E. Apfel, Extension of acoustic levitation to include the study of micron-size particles in a more compressible host liquid, *J. Acoust. Soc. Am.* **71**, 1261 (1982).
- [53] A. E. Kamholz, E. A. Schilling, and P. Yager, Optical measurement of transverse molecular diffusion in a microchannel, *Biophys. J.* **80**, 1967 (2001).
- [54] M. Godin, A. K. Bryan, T. P. Burg, K. Babcock, and S. R. Manalis, Measuring the mass, density, and size of particles and cells using a suspended microchannel resonator, *Appl. Phys. Lett.* **91**, 1 (2007).
- [55] S. Karthick and A. K. Sen, Improved understanding of the acoustophoretic focusing of dense suspensions in a microchannel, *Phys. Rev. E* **96**, 1 (2017).
- [56] R. Silva, P. Dow, R. Dubay, C. Lissandrello, J. Holder, D. Densmore, and J. Fiering, Rapid prototyping and parametric optimization of plastic acoustofluidic devices for blood-bacteria separation, *Biomed. Microdevices* **19**, 70 (2017).
- [57] A. Savitzky and M. J. Golay, Smoothing and differentiation of data by simplified least squares procedures, *Anal. Chem.* **36**, 1627 (1964).